Physica 26D (1987) 321–335
North-Holland, Amsterdam

SUPPRESSION OF PERIOD DOUBLING IN THE DYNAMICS OF A BOUNCING BALL

Kurt WIESENFELD
Physics Department, Brookhaven National Laboratory, Upton, NY 11973, USA

and

Nicholas B. TUFILLARO
Physics Department, Bryn Mawr College, Bryn Mawr, PA 19010, USA

Received 15 July 1986
Revised manuscript received 20 October 1986

We present a theoretical and experimental study of a "bouncing ball" system, where the effect of a near-resonant perturbation is to suppress the onset of the first period doubling bifurcation. Near the bifurcation point, the full dynamical equations are reduced to a discrete-time map governing the dynamics on a slowly oscillating center manifold. The derivation emphasizes the geometry of the phase-space dynamics, and serves to clarify several points of a recently proposed theory regarding the effects of strong near-resonant perturbations. Our experimental results agree with the simple theory for moderate perturbations; for larger perturbations, higher order effects must be included.

1. Introduction

When poised near the onset of a dynamical instability, any physical system becomes sensitive to even small perturbations. This sensitivity has both negative and positive ramifications. In laboratory experiments, the effects of external noise become particularly great near these bifurcation points, leading to new structure in the observed power spectra which obscures the measurements [1–4]. On the other hand, it is possible to take practical advantage of this sensitivity in a simple way to make high-gain parametric amplifiers [5, 6]. For example, *any* T-periodic system which exhibits a period doubling bifurcation at some parameter value $\lambda = \lambda_c$ will amplify coherent signals for λ near λ_c, provided the signal has period close to $2T$ [1, 5]. This fact has been demonstrated in a variety of experiments, using superconducting Josephson junctions [7–9], semiconductor lasers [10], NMR lasers [11], and a mechanical "bouncing ball" system [4].

The theory of small-signal amplification near the onset of dynamical instabilities predicts a simple scaling law for the power gain

$$S(\omega) \sim \frac{\Lambda^2}{\mu^2 + \Delta^2}, \tag{1.1}$$

where Λ is the amplitude of the perturbation, μ is the bifurcation parameter ($\mu \sim \lambda - \lambda_c$), and Δ is the *detuning* frequency (i.e. signal frequency minus half the fundamental). The Lorentzian response law holds for small enough perturbations Λ, but is known to break down for larger perturbations. It was observed [12] that the breakdown of eq. (1.1) coincided with a variety of curious phenomena. In particular, the presence of the signal caused a shift

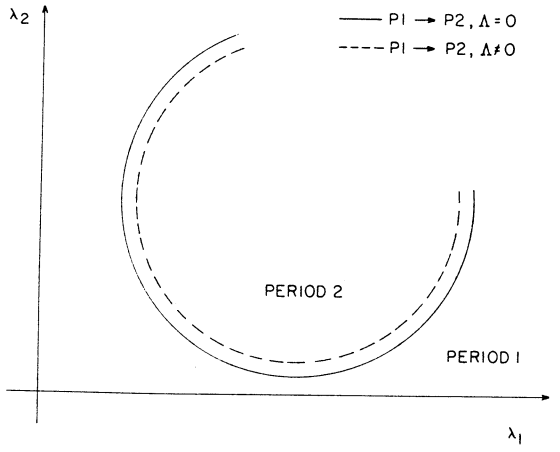

Fig. 1. Schematic representation of the effect of near-resonant perturbations on the onset of period doubling. The solid (dashed) curve represents the points in parameters space λ_1–λ_2 where the period-one solution loses stability in the absence (presence) of the perturbation Λ.

of the bifurcation point λ_* away from the unperturbed value λ_c. Remarkably, the shift was always such as to *stabilize* the system, as depicted schematically in fig. 1. [This observation pertains specifically to nonautonomous systems which are in addition externally perturbed, so that frequency-locking phenomena are automatically ruled out.] By turning on the perturbation, it was possible to drive a system from the period doubled state to the undoubled stated (P2 → P1), but not vice versa. The suppression of period doubling via near-resonant perturbation has also been observed in experiments on magnetostrictive ribbons [13] and in digital simulations of the driven damped pendulum equation [14].

The bifurcation shift was explained by a simple theory [12] that was motivated by the notions of the Center Manifold Theorem and normal forms familiar from bifurcation theory [15–17]. Essentially, it was argued that the crucial dynamics were captured by the first-order ODE

$$\dot{x} = \mu x - x^3 + \Lambda \cos \Delta t, \tag{1.2}$$

where the scalar $x(t)$ represents a slowly varying envelope function for the full (vector) dynamical variable $\boldsymbol{X} \in R^N$. In fact, by studying the reduced eq. (1.2), not only can one explain the power law shift of the bifurcation point

$$\mu_* \sim \frac{\lambda_* - \lambda_c}{\lambda_c} \propto \Lambda^{2/3} \tag{1.3}$$

but also all of the other observed phenomena associated with strong, near-resonant perturbations [12].

The main purpose of this paper is to clarify the origin of the "normal form" eq. (1.2) and the underlying dynamical picture, by explicitly reducing the full perturbed dynamics of a specific physical system, namely a ball bouncing on a vibrating table [4, 18–25]. We show that eq. (1.2) is the continuous-flow approximation to a one-dimensional discrete map; moreover, we can explain both qualitatively and quantitatively the observational fact [12] that successive iterates of the Poincaré return map lie on highly eccentric ellipses, rather than along a (curved) line-segment. We also present experimental results for the bouncing ball system, testing two of the predictions of ref. 12, namely the bifurcation shift law (1.3) and the curious "squaring" effect of the output as the detuning Δ is diminished.

2. Background

In this section we review the essential dynamical features of a resonantly perturbed system near the onset of period doubling. The situation is depicted in fig. 2. We assume that there is a stable T-periodic solution $\boldsymbol{X}_0(t) \in R^N$ to the unperturbed dynamical system. This implies that there is a closed orbit in phase space, as illustrated in fig. 2a. We assume this orbit undergoes a supercritical period doubling bifurcation at parameter value $\lambda = \lambda_c$.

The effect of a periodic perturbation can be understood best by considering first the response to an impulse perturbation. Suppose the system is kicked off of the limit cycle to the point $\boldsymbol{q}_0$:

subsequently, the trajectory through q_0 relaxes back toward X_0. This trajectory will intersect the section P transverse to X_0 at points $q_1, q_2, \ldots$, asymptotically approaching $q_\infty = X_0 \cap P$. Since the phase space is N-dimensional, the section P is $(N-1)$-dimensional. In general, the $\{q_i\}$ will approach q_∞ in some haphazard way, with no discernable pattern. However, for parameter values λ near λ_c, a tremendous simplification takes place (fig. 2b): after the first few intersections, all of the q_i fall on a (nearly straight) one-dimensional curve; moreover, the q_i approach q_∞ in the alternating fashion shown. (This is precisely the reason that the period doubling bifurcation is also called the "flip" bifurcation.)

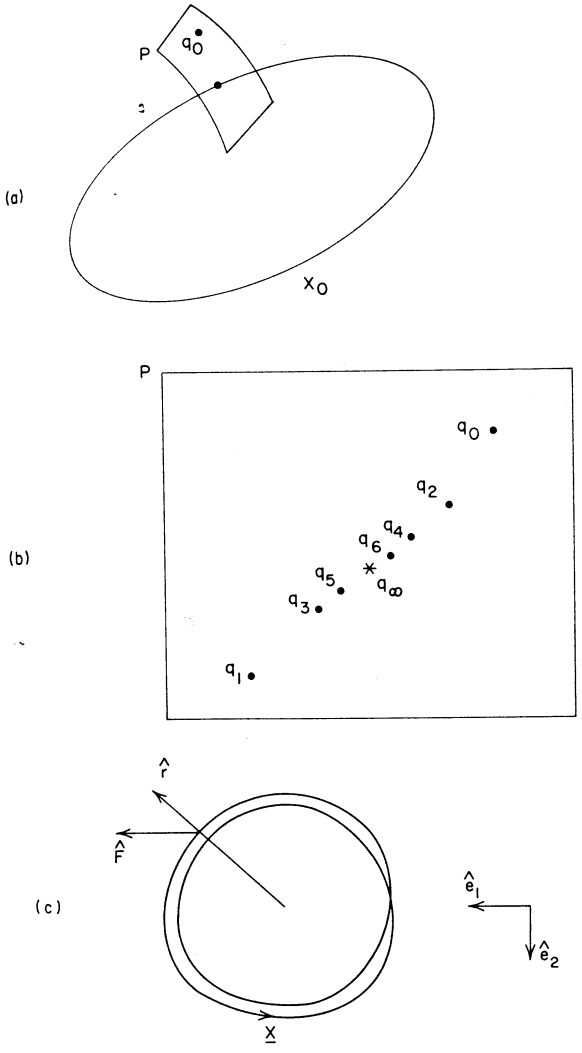

Fig. 2. Phase-space dynamics. (a) Unperturbed orbit X_0 cut by transverse section P. Far from bifurcation, orbit through q_0 relaxes toward $q_\infty = X_0 \cap P$ in a haphazard way. (b) Near period doubling, q_i quickly collapse to the one-dimensional center manifold, then approach q_∞ in an alternating fashion. (c) Projection of transient orbit. Average near-resonant perturbation over time $2T$ contributes term at beat frequency Δ, as described in the text.

Why is it that the dynamics of P effectively reduce from $N-1$ to 1 dimension near the bifurcation point? In general, one can assign a set of relaxation rates ρ_n, one for each (independent) direction in phase space. Near the bifurcation point, one of these rates tends to zero, so that *asymptotically* orbits approach q_∞ along the corresponding "eigendirection." The crucial point is that, when a continuous-time perturbation is present, the system's response is dominated by the dynamics along this slow-relaxing direction [2, 5].

Going back to the phase trajectory that generates the $\{q_i\}$, we see that for λ near λ_c, the transient orbit slowly spirals into X_0 with period *twice* T, owing to the flip behavior. By analogy with linear oscillators, we anticipate that – in the presence of a *periodic* perturbation – there will be resonance phenomena for perturbations with period close to $2T$. This resonance behavior is easy to observe experimentally, and has been reported in studies using electrical circuits [5, 12], NMR lasers [11] magnetostrictive ribbons [13], and the bouncing ball system [4]. The theory is essentially a nonlinear dynamical perspective on parametric amplification, and one can ask whether previous experiments demonstrating parametric amplification are related to this picture. Sure enough, the high-gain parameter values for superconducting Josephson junction parametric amplifiers [7–9, 26, 27] and semiconductor sideband parametric amplifiers [10] are very close to the parameter values for the onset of bifurcations (either period doubling [7–10] or saddle-node bifurcations [26, 27]). More recently, small-signal amplification has been observed near the onset of a Hopf bifurcation in the electrical conductivity of barium–sodium–niobate single crystals [28].

There is a nice "geometric" way to understand why the perturbation at frequency $\omega_1 \approx \pi/T$ gives rise to a resonant response having a characteristic time-scale at the *beat frequency* $\Delta = (\frac{1}{2}\omega_0 - \omega_1)$. The idea [29] is to look at the transient (unperturbed) trajectory that generates fig. 2b – this orbit $\boldsymbol{X}$ is essentially a slightly modulated circular trajectory (see fig. 2c)

$$\boldsymbol{X} = \left[r + \varepsilon \cos\left(\tfrac{1}{2}\omega_0 t\right)\right]\hat{\boldsymbol{r}};$$
$$\hat{\boldsymbol{r}} = \cos\omega_0 t\,\hat{\boldsymbol{e}}_1 + \sin\omega_0 t\,\hat{\boldsymbol{e}}_2,$$

where the modulation frequency is $\frac{1}{2}\omega_0$ due to the proximity of the flip bifurcation. We have neglected the (slow) decay of the amplitude ε. The periodic perturbation $\boldsymbol{F}$ is taken to be a vector of constant direction $\hat{\boldsymbol{e}}_1$:

$$F = \lambda \cos\left(\frac{\omega_0}{2} + \Delta\right) t\,\hat{\boldsymbol{e}}_1.$$

We compute the effect of the perturbation averaged over the time-interval $2T$:

$$\frac{1}{2T}\int_{t_0}^{t_0+2T} \boldsymbol{X}\cdot\boldsymbol{F}\,\mathrm{d}t = \frac{\lambda}{2T}\int_{t_0}^{t_0+2T}\left(r + \varepsilon\cos\frac{\omega_0}{2}t\right)$$
$$\times \cos\omega_0 t \cos\left(\frac{\omega_0}{2} + \Delta\right) t\,\mathrm{d}t.$$

For small Δ, we can treat $\cos\Delta t$ as constant over the range of integration, with the result

$$\frac{1}{2T}\int_{t_0}^{t_0+2T} \boldsymbol{X}\cdot\boldsymbol{F}\,\mathrm{d}t = \frac{\lambda\varepsilon}{2}\cos\Delta t_0.$$

This notion of averaging the dynamics over two periods of the unperturbed orbit corresponds to looking at the second iterate of the return map, and will recur at the end of section 3. A similar averaging procedure was employed in the original derivation of eq. (1.2) [12].

The theory of perturbed dynamical systems is particularly simple in the vicinity of a simple (i.e. codimension-one) bifurcation. This is because the crucial dynamics is typically low-dimensional near criticality – indeed, the number of relevant phase-space dimensions depends on the *class* of instability involved, rather than the (possibly large) number of dimensions of the full phase space. For the case of period doubling, the dynamics reduce to a one-dimensional map (fig. 2b); for a periodic orbit undergoing a Hopf instability – typically leading to motion on an invariant 2-torus – the return map dynamics reduce to a two-dimensional manifold; and so forth. This low-dimensional manifold is the so-called *center manifold*, and the mathematics behind the effective reduction of diemsnion at the bifurcation point is contained in the Center Manifold Theorem [15–17].

[The idea that the slow-relaxing variables are key in determining the dynamics of a system is familiar to laser physicists, under the rubrik of "adiabatic elimination", enunciated by Haken [30]. The procedure finds its formal mathematical counterpart in the Center Manifold Theorem, and related developments [15–17].]

The sequence of steps leading from an N-dimensional "flow" (i.e. generated by an ODE for $N < \infty$, by a PDE otherwise) is illustrated schematically in fig. 3, for the case where the center manifold is one-dimensional, as in the period doubling situation. The techniques for calculating the appropriate reduced dynamics are well-known [15–17], though as a rule explicit construction of the $(N-1)$-dimensional return map is difficult to achieve, especially for physically realizable systems. Happily, the bouncing ball system is an exception to this rule.

One would like to carry out this reduction procedure in the presence of a near-resonant forcing, by introducing the perturbation to the full N-dimensional dynamical equations. What was achieved in ref. 12 was to start with the one-dimensional map of the *unperturbed* system, and introduce "by hand" the appropriate perturbation and nonlinear terms at that level. By employing an averaging method, the second iterate of this map was approximated by the first order flow, eq. (1.2).

The strength of the analysis of ref. 12 is that it was based on general properties of phase-space dynamics and geometry of period doubling orbits.

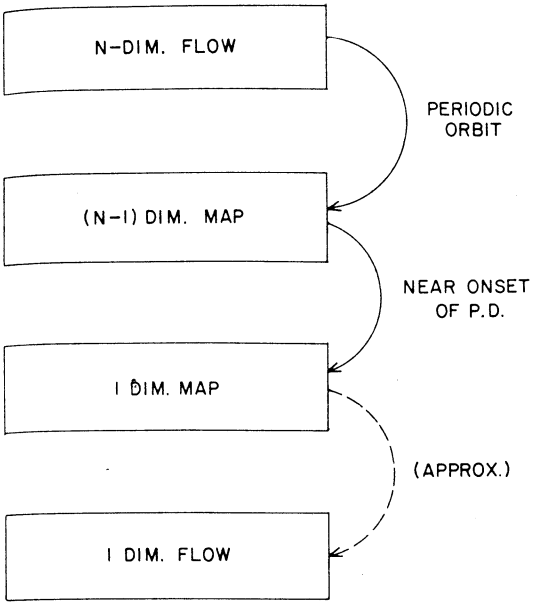

Fig. 3. Rigorous reduction scheme from N-dimensional flow to one-dimensional map. The "normal form" eq. (1.2) is attained by an approximation to the second iterate of the center manifold map.

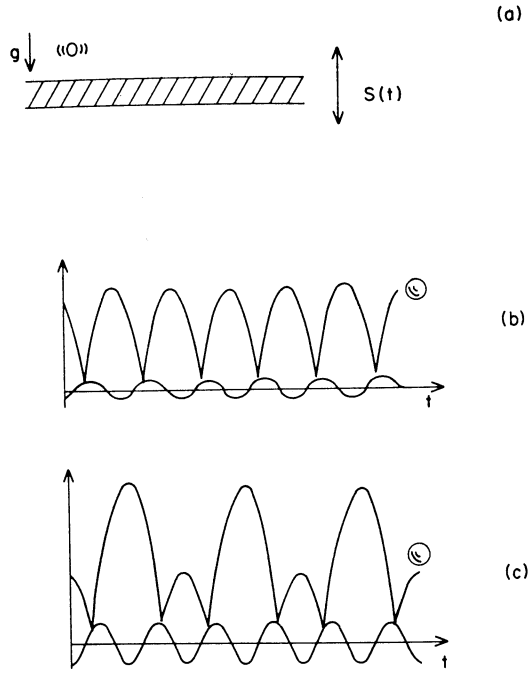

Fig. 4. The bouncing ball system. (a) Ball bounces vertically on a table oscillating at two frequencies: $s(t) = A \sin \omega_0 t + B \sin(\omega_s t + \phi)$, $A \gg B$. (b) Unperturbed ($B = 0$) period-one solution: ball impacts table at same phase each bounce. (c) Unperturbed period-two solution: ball alternates between high and low bounces.

The calculation in the next section is both more and less ambitious: though carrying out the complete reduction scheme of fig. 3, it focuses on a specific dynamical system. Since we recover eq. (1.2), we suspect that a general derivation of eq. (1.2) is possible.

3. Center manifold reduction for the bouncing ball

In this section, we consider the specific dynamical system illustrated in fig. 4a. A ball, constrained to move vertically in a gravitational field, bounces on a vibrating table with height $s(t) = A \cos \omega_0 t + B \cos(\omega_s t + \phi)$. The collisions are not perfectly elastic, but are characterized by a coefficient of restitution α, $0 < \alpha < 1$. [This system with $\alpha = 1$ is a modification due to Pustylnikov [31] of a model introduced by Fermi [32] representing cosmic ray accelerations.] This "bouncing ball" system has been studied by a number of people [18–25] for the case in which the table oscillates at a single frequency ω_0. Pieranski and Malecki have also studied the case of two frequencies [4], which is directly relevant to the problem treated here.

Consider first the "unperturbed problem", with $B = 0$. For fixed ω_0, there is a range of amplitudes $A \in (A_0, A_1)$ for which the ball executes equal-height bounces with frequency ω_0, as illustrated in fig. 4b. Physically, the bounce occurs with the upward bound table, and the ball gains just enough energy to offset that lost by the inelastic collision. As A is increased beyond A_1, there is a period doubling bifurcation: the ball makes alternatively high and low bounces, so that its motion repeats with frequency $\omega_0/2$. For still higher A, further period doublings occur, leading to chaos; but we want to focus on parameter values in the vicinity of the first period doubling, $A \approx A_1$.

This dynamical system has the rather unusual properties that (i) the periodic solution for $A \in$

(A_0, A_1) can be explicitly constructed, and (ii) the Poincaré return map can be analytically developed from the governing differential equations. These features make this an ideal system to carry out the proposed center manifold reduction.

The dynamical state of the bouncing ball system is specified by three variables: the ball's height x, its velocity v, and the time t (which specifies the table's vertical position $s(t)$). Let t_k be the time of the kth table-ball collision, and v_k the ball's velocity immediately after the kth collision. Then the system evolves according to two equations:

$$v_k - \dot{s}_k = -\alpha\left[v_{k-1} - g(t_k - t_{k-1}) - \dot{s}_k\right], \tag{3.1}$$

$$s_k = s_{k-1} + v_{k-1}(t_k - t_{k-1}) - \tfrac{1}{2}g(t_k - t_{k-1})^2, \tag{3.2}$$

where $s_k = s(t_k)$. The first of these is the so-called impact relation, which states that the relative ball-table speed just after the kth collision is a fraction α of its value just before the kth collision. (The overdot denotes differentiation with respect to time.) Eq. (3.2) determines t_k – given t_{k-1} – by equating the table position and ball position at t_k: specifically, t_k is the smallest solution of eq. (3.2) such that $t_k > t_{k-1}$.

Note that we have already passed to a discrete-time map in eqs. (3.1), (3.2), in effect having integrated Newton's 2nd Law for the ball between impacts.

It is convenient to introduce an approximation at this point: we suppose that the table's oscillation amplitude is much smaller than the ball's maximum height. Then, eqs. (3.1), (3.2) become

$$t_k = \frac{2}{g}v_{k-1} + t_{k-1} \tag{3.3}$$

and

$$v_k = \alpha v_{k-1} + (1+\alpha)\dot{s}_k. \tag{3.4}$$

(The ensuing derivation can be carried out without making this "high-bounce" approximation; however, the expressions thus obtained are far more cumbersome, and add no insight to the essential geometry involved.)

We specify the table's position to be the sum of a large oscillation and a small oscillation

$$s(t) = A\sin\omega_0 t + B\sin(\omega_s t + \phi), \quad B \ll A, \tag{3.5}$$

we have in mind the situation where $\omega_s \approx \frac{1}{2}\omega_0$. It is natural to introduce dimensionless time and velocity variables,

$$\tau \equiv \omega_0 t; \quad w \equiv \frac{2\omega_0}{g}v,$$

in terms of which eqs. (3.3), (3.4) become

$$\tau_k = w_{k-1} + \tau_{k-1}, \tag{3.6}$$

$$w_k = \alpha w_{k-1} + \Gamma\cos\tau_k + \Lambda\cos(\Omega\tau_k + \phi), \tag{3.7}$$

where

$$\Gamma \equiv \frac{2\omega_0^2}{g}(1+\alpha)A; \quad \Lambda \equiv \frac{2\omega_0\omega_s}{g}B; \quad \Omega \equiv \frac{\omega_s}{\omega_0}.$$

The derivation that follows is divided into two parts. First, the unperturbed system ($\Lambda = 0$) is analyzed: we find the bifurcation point Γ_c, determine the center manifold dynamics precisely at Γ_c, and then *unfold* the dynamical equation so that it is valid in a range of parameter values Γ around Γ_c. All of these steps are standard [15]. The second part allows for the presence of a small perturbation ($\Lambda \neq 0$) at frequency $\Omega \approx 1/2$, and the same analysis is carried through. We show that the perturbation alters the reduced dynamics in two essential ways: the dynamics along the center manifold are driven by a time-dependent term, and the center manifold itself is now explicitly time-dependent. Although this last feature of a time-varying center manifold is not standard, it follows naturally and is consistent with the reduction procedure.

3.1. *The unperturbed system* ($\Lambda = 0$)

We begin by finding the first period doubling bifurcation of the unperturbed system. It is a

simple matter to find the period-one solution (τ_k^*, w_k^*): the ball bounces once per table oscillation, so $\tau_k - \tau_{k-1} = 2\pi$, or

$$\tau_k^* = 2\pi k + \tau_0^*. \tag{3.8}$$

From eq. (3.6), this implies

$$w_k^* = 2\pi. \tag{3.9}$$

As expected, taking time τ modulo 2π, the periodic solution is a fixed point of the discrete mapping. The constant τ_0^* follows from eqs. (3.9) and (3.7),

$$\tau_0^* = \arccos\left[\frac{2\pi(1-\alpha)}{\Gamma}\right]. \tag{3.10}$$

Now look at the dynamics near this solution. Let

$$\tau_k^* = 2\pi k + \tau_0^* + a_k,$$
$$w_k = w^* + b_k,$$

with a_k and b_k regarded as small. Substitution of these into eqs. (3.6), (3.7) gives evolution equations for a_k, b_k:

$$\begin{pmatrix} a_{k+1} \\ b_{k+1} \end{pmatrix} = \begin{pmatrix} 1 & 1 \\ -\Gamma \sin\tau^* & \alpha - \Gamma\sin\tau^* \end{pmatrix}\begin{pmatrix} a_k \\ b_k \end{pmatrix} + \begin{pmatrix} 0 \\ -\frac{\Gamma}{2}\cos\tau_0^*(a_k+b_k)^2 + \frac{\Gamma}{6}\sin\tau_0^*(a_k+b_k)^3 \end{pmatrix} + \mathcal{O}(4), \tag{3.11}$$

where $\mathcal{O}(4)$ stands for terms quartic and higher in a_k, b_k.

The stability of the period-one solution is determined by the linear part of eq. (3.11). A period doubling bifurcation occurs when one of the eigenvalues of the matrix is -1. For fixed α, this occurs when Γ reaches its critical value

$$\Gamma_c = \frac{2(1+\alpha)}{\sin\tau_0^*}. \tag{3.12}$$

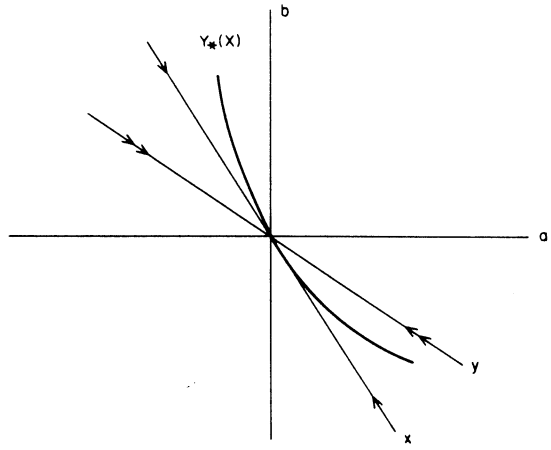

Fig. 5. Transformed coordinates $(a, b) \to (x, y)$. Dynamics relax rapidly in the y-direction toward the center manifold $y_*(x)$. Dynamics evolve slowly along the center manifold, which is tangent to the x-axis at the origin.

The next step is to make a linear change of variables such that, at the bifurcation point Γ_c, the linearized dynamics is diagonal. This is readily achieved, with the result

$$\begin{pmatrix} x_{k+1} \\ y_{k+1} \end{pmatrix} = \begin{pmatrix} -1 & 0 \\ 0 & -\alpha \end{pmatrix}\begin{pmatrix} x_k \\ y_k \end{pmatrix} + \begin{pmatrix} -g_k \\ +g_k \end{pmatrix} + \mathcal{O}(4), \tag{3.13}$$

$$g_k = (\alpha-1)^{-1}\left[\frac{\Gamma_c}{2}\cos\tau_0^*(x_k+\alpha y_k)^2 + \frac{\Gamma_c}{6}\sin\tau_0^*(x_k+\alpha y_k)^3\right], \tag{3.14}$$

$$S\begin{pmatrix} x_k \\ y_k \end{pmatrix} = \begin{pmatrix} a_k \\ b_k \end{pmatrix}, \tag{3.15}$$

the transformation matrix S being given by

$$S = \begin{pmatrix} 1 & 1 \\ -2 & -1-\alpha \end{pmatrix}. \tag{3.16}$$

The important point here is that, to linear approximation, trajectories evolve quickly toward the line $y = 0$, and are neutrally stable along the x-axis, (i.e. at the bifurcation point, the dynamics along

the center manifold are governed entirely by nonlinear terms). This is illustrated schematically in fig. 5. Note that the "eigendirections" x and y are not orthogonal (see eq. (3.15)).

When we include the nonlinear terms, we find that trajectories collapse quickly to a center manifold which is tangent to the x-axis at the origin. A power series expression for the center manifold $y_*(x)$

$$y_*(x_k) = cx_k^2 + dx_k^3 + \mathcal{O}(4) \tag{3.17}$$

can be developed as follows. The fast-relaxing dynamics is governed by (see eq. (3.13))

$$\Delta y \equiv y_{k+1} - y_k = -(1+\alpha)y_k + g_k(x, y) + \mathcal{O}(4). \tag{3.18}$$

On the center manifold, $\Delta y = 0$, so that

$$0 = -(1+\alpha)y_*(x_k) + g_k(x_k, y_*(x_k)) + \mathcal{O}(4). \tag{3.19}$$

It is a straightforward matter to determine the coefficients c and d, by combining eqs. (3.14), (3.17), and (3.19):

$$c = \cot \tau_0^*/(\alpha - 1), \tag{3.20}$$

$$d = 2\alpha c^2 + (3\alpha - 3)^{-1}. \tag{3.21}$$

Substitution of eq. (3.17) into eq. (3.13) yields an equation for the slowly-evolving dynamics along the center manifold

$$x_{k+1} = -x_k - g_k(x_k, y_*(x_k)) + \mathcal{O}(4),$$

so that

$$x_{k+1} = -x_k + px_k^2 + qx_k^3 + \mathcal{O}(4), \tag{3.22}$$

where

$$p = (1+\alpha)\cot \tau_0^*/(1-\alpha)$$

and

$$q = \frac{1+\alpha}{1-\alpha}\left[\frac{1}{3} - \frac{2\alpha \cot^2 \tau_0^*}{1-\alpha}\right].$$

Observe that the coefficients in eq. (3.22) depend on the value of c, but not on d – that is, only the quadratic behavior of the center manifold effects the dynamics along the center manifold, to this order.

Eq. (3.22) holds precisely at the bifurcation point $\Gamma = \Gamma_c$. The final step is to extend the analysis to values of Γ not quite equal to Γ_c, but nearly so. To do this, introduce the small "unfolding parameter" μ, such that

$$\Gamma - \Gamma_c = \left(\frac{\alpha - 1}{\sin \tau_0^*}\right)\mu, \tag{3.23}$$

with $\mu \sim \mathcal{O}(2)$. (The factor in parentheses is simply for notational convenience.) We proceed exactly as in the case of $\Gamma = \Gamma_c$; the Poincaré dynamics in the (x_k, y_k) coordinate plane is now

$$\begin{pmatrix} x_{k+1} \\ y_{k+1} \end{pmatrix} = \begin{pmatrix} -1+\mu & \alpha\mu \\ -\mu & -\alpha - \alpha\mu \end{pmatrix}\begin{pmatrix} x_k \\ y_k \end{pmatrix} + \begin{pmatrix} -\tilde{g}_k \\ \tilde{g}_k \end{pmatrix} + \mathcal{O}(4), \tag{3.24}$$

where $\tilde{g}_k$ is given by eq. (3.14) with Γ_c replaced by Γ. The center manifold y_* is now a function of both x_k and μ, and can be expanded as the power series

$$y_*(x_k, \mu) = cx_k^2 + c'\mu + dx_k^3 + d'\mu x_k + \mathcal{O}(4). \tag{3.25}$$

The coefficients are determined by substitution of (3.25) into the second component of (3.24), and setting $y_{k+1} - y_k = \mathcal{O}(4)$ on the center manifold. One finds

$$c' = 0, \quad d' = -(\alpha + 1)^{-1}, \tag{3.26}$$

and c, d given by eqs. (3.20) and (3.21), respectively. Finally, evaluating the equation for x_{k+1} in (3.24) on the center manifold yields

$$x_{k+1} = -(1+\mu)x_k + px_k^2 + qx_k^3 + \mathcal{O}(4), \tag{3.27}$$

which differs from (3.2) solely by the linear term μx_k. (Note that the coefficients p and q can still be evaluated at the bifurcation point; the unfolding leads to higher order corrections only.) The reason why μ is properly an $\mathcal{O}(2)$ quantity is clear if one computes the second iterate of eq. (3.27):

$$x_{k+2} = (1+2\mu)x_k - 2(p^2+q)x_k^3 + \mathcal{O}(4). \tag{3.28}$$

Thus, the terms quadratic in x_k cancel exactly, so that a balance between the (unfolded) linear term and the dominant nonlinear term is achieved for $\mu \sim \mathcal{O}(2)$.

One final remark before proceeding to the perturbed calculation. Eqs. (3.27), (3.28) illustrate the familiar point that, if one wants to pass from a discrete mapping to a continuous time approximation near a period doubling bifurcation, it is the second iterate that should be modified, rather than the first iterate. Of course, when eq. (3.27) undergoes a period doubling, eq. (3.28) describes a symmetry-breaking (or pitchfork) bifurcation.

3.2. *The perturbed system* ($\Lambda \neq 0$)

We can carry out an entirely parallel analysis in the presence of the perturbation at frequency Ω. Eq. (3.11) is modified by the addition to the right-hand side of a nonautonomous term:

$$\begin{pmatrix} 0 \\ \Lambda \cos\left[\Omega(\tau_0^* + 2\pi k + a_k + b_k) + \phi\right] \end{pmatrix}. \tag{3.29}$$

As we have seen in eq. (3.28), the dominant nonlinear contribution to the 2nd-iterate dynamics on the center manifold is cubic, which sets the scale for the balanced competition between linear and nonlinear terms. We want the leading contribution of the perturbation to also be of this order: this means that $\Lambda \sim \mathcal{O}(3)$, and so expression (3.29) reduces to

$$\begin{pmatrix} 0 \\ \Lambda \cos\left[\Omega(\tau_0^* + 2\pi k) + \phi\right] \end{pmatrix} + \mathcal{O}(4).$$

In terms of the eigenbasis x_k, y_k, the dynamical equations become (see eq. (3.13))

$$\begin{pmatrix} x_{k+1} \\ y_{k+1} \end{pmatrix} = \begin{pmatrix} -1 & 0 \\ 0 & -\alpha \end{pmatrix} \begin{pmatrix} x_k \\ y_k \end{pmatrix} + \begin{pmatrix} -g_k \\ g_k \end{pmatrix} + \Lambda \begin{pmatrix} -\xi_k \\ \xi_k \end{pmatrix}, \tag{3.30}$$

where

$$\xi_k = \frac{\cos\left[\Omega(\tau_0^* + 2\pi k) + \phi\right]}{1-\alpha}. \tag{3.31}$$

We turn next to the determination of the center manifold y_*. From the fast-relaxing dynamics, we set (compare eq. (3.19))

$$0 = -(1+\alpha)y_*(x_k) + g_k(x_k, y_*(x_k)) + \Lambda\xi_k + \mathcal{O}(4). \tag{3.32}$$

We can satisfy eq. (3.32), *provided we allow* y_* *to depend explicitly on* k:

$$y_* = cx_k^2 + dx_k^3 + e_k + \mathcal{O}(4). \tag{3.33}$$

Combining eqs. (3.14), (3.31)–(3.33) yields the same expressions for the coefficients c and d as before (eqs. (3.20), (3.21)), and

$$e_k = (1+\alpha)^{-1}\Lambda\xi_k, \tag{3.34}$$

so that the center manifold just oscillates at the perturbation frequency. We will return to this effect at the end of the section.

The slow dynamics along the center manifold follows from eqs. (3.33) and (3.30):

$$x_{k+1} = -(1+\mu)x_k + px_k^2 + qx_k^3 - \Lambda\xi_k + \mathcal{O}(4), \tag{3.35}$$

where p and q are the same as for the unperturbed problem, and we have included the unfolding parameter μ, as before. Note that this equation does not depend on the $\mathcal{O}(3)$ pieces of the center

manifold – that is, the fact that the center manifold depends on time does not affect the dynamics along the center manifold.

Finally, we look at the second iterate of eq. (3.35):

$$x_{k+2} = (1+2\mu)x_k - 2(p^2+q)x_k^3 + \Lambda(\xi_k - \xi_{k+1}). \tag{3.36}$$

Up until now, no restriction has been replaced on the perturbation frequency Ω. At this point, we take $\Omega = 1/2 + \Delta$, with $\Delta \sim \mathcal{O}(1)$. It follows that

$$\begin{aligned}\xi_k - \xi_{k+1} &= \{\cos[\Omega(\tau_0^* + 2\pi k) + \phi] \\ &\quad - \cos[\Omega(\tau_0^* + 2\pi k + 2\pi) + \phi]\}/(1-\alpha) \\ &= (-)^k \cdot 2\cos(2\pi\Delta k + \Omega\tau_0^* + \phi)/(1-\alpha).\end{aligned}$$

Consequently, the forcing term $\Lambda(\xi_k - \xi_{k+1})$ in eq. (3.36) has the *beat* frequency Δ. Moreover, the overall sign of this term is negative for odd iterates, and positive for even iterates. If we pass to the continuous-time approximation of the second iterate,

$$\frac{x_{k+2} - x_k}{4\pi} = \frac{\Delta x}{\Delta t} \to \dot{x},$$

and translate the time origin, we recover the so-called normal form [12] eq. (1.2), up to simple rescalings

$$\dot{x} = \left(\frac{\mu}{\pi}\right)x - \left(\frac{p^2+q}{\pi}\right)x^3 + \frac{\Lambda}{\pi(1-\alpha)}\cos\Delta t. \tag{3.37}$$

We close this section with two remarks. First, note that because the oscillations of the center manifold superpose with the periodic trajectories along the center manifold, iterates of the return map fall on an (elongated) ellipse on the x–y plane. In fact, since the two frequencies (parallel and perpendicular to the center manifold) are the same, the iterates form a discrete set of points that do not fill in the ellipse. Moreover, our analysis leads to a new prediction regarding the way the major and minor axes scale with bifurcation parameter μ. The center manifold oscillates with amplitude $\delta_\perp$ of order Λ (see eqs. (3.33, 34), while the maximum displacement along the center manifold $\delta_\parallel$ is order Λ/μ (see eq. (3.37)). The prediction for the expected *aspect ratio* R is thus

$$R \equiv \frac{\delta_\parallel}{\delta_\perp} \sim 1/\mu. \tag{3.38}$$

(In an N-dimensional system, all $N-1$ minor axes of the Poincaré hyperellipsoid should scale as $\delta_\perp$.)

The second remark is that the most basic prediction of eq. (3.37) – the shift of the period doubling bifurcation point – is easily obtained by the following heuristic argument. Essentially, the unperturbed bifurcation point $\mu = 0$ is shifted to $\mu = \mu_*$ – the bifurcation occurs when there is a balanced competition between the three terms on the right-hand side:

$$|\mu_* x| \sim |x^3| \sim |\Lambda\cos\Delta t|,$$

so that $\mu_* \sim |x^2|$, $\Lambda \sim |x^3|$, and thus

$$\mu_* \sim \Lambda^{2/3}. \tag{3.39}$$

4. Experimental set-up and results

In this section, we report measurements checking the prediction eq. (1.3), regarding the degree to which near-resonant perturbations suppress the onset of period doubling. We also demonstrate the curious qualitative effect of the "squaring" of the output as the perturbation amplitude grows. Both effects are easily observed in a bouncing ball apparatus constructed with an ordinary loud speaker, function generator, and ball bearing. Pieranski [19] appears to be the first to construct this simple mechanical system. Our apparatus includes two improvements: we employ a piezoelectric film as a detector, and also some additional digitizing electronics.

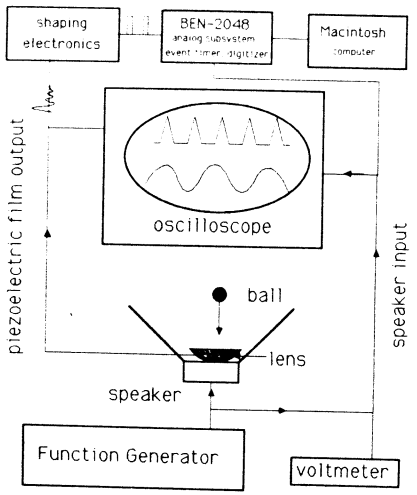

Fig. 6. Experimental realization of the bouncing ball machine.

An experimental realization of the bouncing ball machine is depicted in fig. 6. A 12″ audio speaker, driven by a function generator (Wavetek model 182A), serves as the vibrating table. For two frequency work, the output of two function generators is summed and then supplied to the speaker [33]. A small ball (between 1/4″ and 5/8″) bounces on a concave lens glued to the speaker – the curvature of the lens helps keep the ball's motion vertical. Fastened to the top surface of the lens is a thin piezoelectric film that generates a voltage spike every time the ball hits the lens [34]. The voltage spike is monitored on an oscilloscope to detect period doubling and other types of bifurcations. The forcing frequency is read from a frequency meter connected to the function generator. Similarly, the relative forcing amplitude can be read from a voltmeter. The output from the piezoelectric film is processed by shaping electronics that generate a logic level pulse at each impact between the ball and the lens. The shaping electronics can also be used to plot strange attractors on a storage oscilloscope as described in a previous publication [22]. The logic level pulses are then set to a commercially available event timer and digitizer that are part of the Bench Top series, a real-time data acquisition system for the Macintosh computer [35]. The Bench Top analog subsystem records the time between pulses in microseconds and stores a permanent record of the time-series on the Macintosh.

It is often desirable to measure the actual amplitude of the speaker's oscillation. This is done by mounting a micrometer across the top of the speaker so that the tip of the micrometer lightly impacts with the lens (the impacts are easily detected by the piezoelectric film). By gently sliding the micrometer vertically and looking for the initial impact between the tip and the lens, it is possible to determine the speaker's actual amplitude and phase of oscillation. Typical speaker oscillation amplitudes are between 0.01 and 2 mm.

Often times the apparatus exhibits what we call a "rolling instability." Instead of moving in the vertical direction, the ball sometimes tends to roll slightly back and forth, exciting motion in the horizontal direction. This behavior can be minimized and often eliminated by isolating the system from mechanical vibrations and carefully experimenting with lenses of many different curvatures. Our apparatus is located in a very quiet room and the speaker itself sits in a heavy metal case that rests on a vibrationally isolated table. The rolling instability can be difficult to eliminate at times, but once removed the system appears to be truly one-dimensional. Also, the piezoelectric film, being essentially a capacitive device, is very sensitive to 60 Hz and other stray pick-up. However, simply grounding the piezoelectric film output to the speaker case appears to remove this noise source.

The onset of period doubling is defined as the point at which the power spectrum first shows a peak at frequency $\frac{1}{2}\omega_0$. An equivalent signature – and the one used here – can be found by monitoring directly the time-intervals $T_n \equiv \tau_n - \tau_{n-1}$ for successive n. In the absence of the perturbation, such a time-series would fall on a single horizontal line below the bifurcation point, and on a pair of horizontal lines after the bifurcation (see the dashed lines of figs. 7a and 7b, respectively). With the perturbation turned on, the subcritical time-

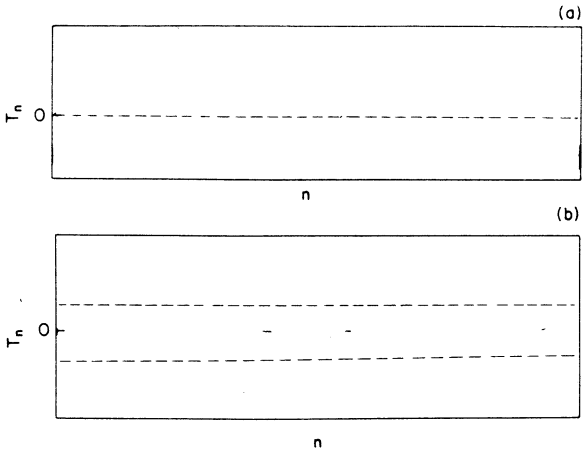

Fig. 7. Experimental time-series of intervals $T_n \equiv \tau_n - \tau_{n-1}$ versus n. (a) Before the bifurcation point: odd-n iterates fall on a slowly oscillating envelope, which is symmetric about $T_n = 0$. Ditto for even-n iterates. (b) After period doubling: slowly oscillating envelopes are no longer symmetric about $T_n = 0$.

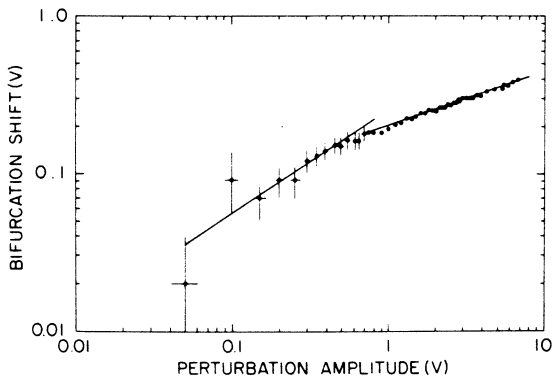

Fig. 8. Experimental results for the bifurcation shift. For smaller perturbation amplitudes, the shift fits a power-law with exponent 0.67 ± 0.07, while for larger amplitudes, the data fits to an exponent of 0.33 ± 0.02.

series shows a modulation about the single line (see the dotted line of fig. 7a): the even-n iterates fall on a slowly-varying envelope of frequency Δ, as do the odd-n iterates. Each of these slowly-varying curves is *symmetric* about its mean value. In contrast, the post-critical (i.e. period-doubled) time-series fall on two slowly-varying curves which are *not symmetric* with respect to the mean value of T_n (fig. 7b). A moment's reflection reveals that this is an example of a well-known fact: a period-doubling of an iterative map corresponds to a symmetry-breaking of the second-iterate map.

To test the power law, eq. (1.3), we need to measure the amplitude A of the forcing oscillator and the perturbation amplitude B (proportional to Λ) at the bifurcation point. We found it easier to measure the driving voltages to the speaker, rather than the actual oscillation amplitudes at the two frequencies ω_0 and ω_1. We verified experimentally that the driving voltages are directly proportional to the table's displacement amplitudes in the parameter regime considered.

Our results, shown in fig. 8, verified that the perturbation always served to suppress the onset of period doubling. The vertical axis plots the voltage difference $V_* - V_0$ where V_* and V_0 are the critical values for the onset of period doubling in the perturbed and unperturbed system, respectively. The horizontal axis plots the perturbation voltage amplitude. The result indicate two distinct scaling regimes: for small perturbing amplitudes - up to about 4% of the larger driving voltage V_0 - the results are consistent with the 2/3-power law; for somewhat larger perturbations, (5% to 10%), the data fit very well a 1/3-power law

$$\text{shift} \propto (\text{perturbation})^{0.33 \pm 0.02}$$

Although we have no theoretical explanation for this new scaling behavior, we can understand why the 2/3-power law breaks down where it does, as we now describe.

The perturbation theory picture relies on the system being near the onset of a single period doubling bifurcation. As can be seen from fig. 7a, the effect of the near-resonant perturbation is to give the dynamics a slowly-modulated period doubled character, even below the bifurcation point. Now, for large enough perturbations, the observed output can show intervals of period-4 behavior, as well, and even higher-period behavior and chaos. This is illustrated in the experimental time-series of fig. 9, which shows about two full cycles of

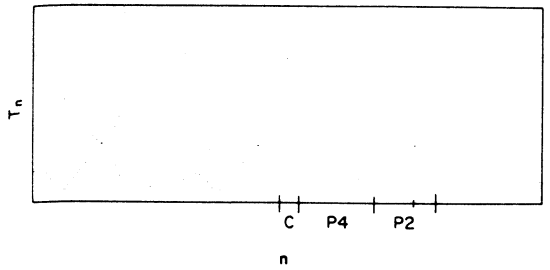

Fig. 9. Digitized time-series from the bouncing ball apparatus of T_n versus n, for perturbation amplitude about 10% of the main drive amplitude. The slowly varying envelope passes through intervals of period-two, period-four, and chaos, then back again. The complete orbit is nonetheless period-one: a power spectrum of this sequence yields no power at frequency $\omega_0/2$. $\omega_0 = 60$ Hz, $\omega_s = 31$ Hz, $B/A = 0.1$.

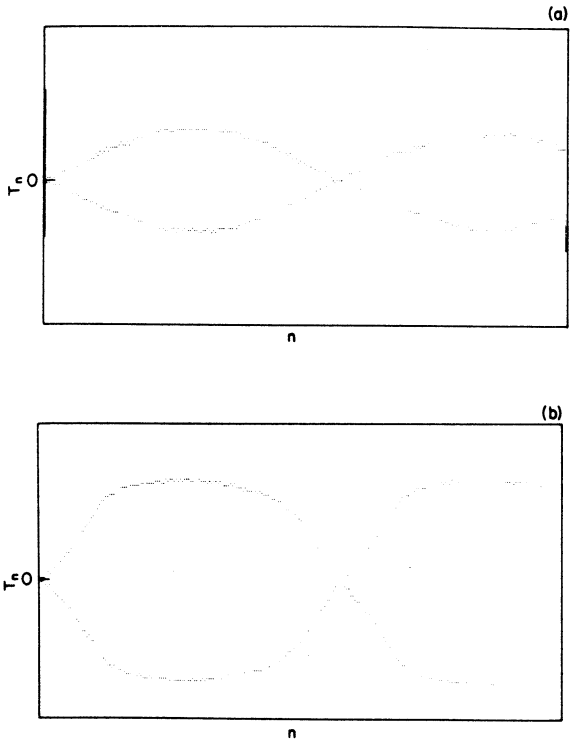

Fig. 10. The "squaring" effect observed in the experimental time-series. (a) For moderate detuning ($\Omega = 0.53$) the slowly varying envelope is nearly sinusoidal. (b) For smaller detuning ($\Omega = 0.51$) the response resembles a square-wave, in addition to being greater in amplitude. The uncertainty in the phase is caused by a rolling instability.

output. During the slow modulation at frequency Δ, the output passes through clearly recognizable intervals of period 2, period 4, and (possibly) chaotic behavior. The deviation in fig. 8 from the 2/3-power law coincides with the onset of these higher-period intervales. This picture suggests two things: first, that the reduced equation (1.2) will be quantitatively valid provided the period doubling bifurcation of the unperturbed system is not too close to the onset of a second bifurcation; second, that the unexpected 1/3-power law for larger perturbations may very well *not* be generic to period doubling systems, insofar as the observed behavior is likely to depend crucially on "global" bifurcation properties of the unperturbed system.

We turn next to the "squaring" effect, which is easily observed in the bouncing ball system. Fig. 10a shows a time-series of a perturbed subcritical orbit with moderate detuning, $(\frac{1}{2}\omega_0 - \omega_1)/\omega_0 \sim 3\%$.] The slowly-varying envelope looks sinusoidal. However, as the detuning is decreased (to about 1%), the output develops a square-wave character, as seen in fig. 10b. This squaring effect is particularly dramatic if one observes directly the return map dynamics (t_n, v_n), eqs. (3.3), (3.4). (In our work, we found it more convenient to monitor a different but equivalent plane, namely the (T_n, T_{n+1}) plane.) In the presence of the perturbation, one observes two points – corresponding the odd-n and even-n iterates of fig. 7a – which move slowly, on the time-scaling of the detuning frequency Δ. For moderate detunings, the two points rhythmically pass through one another. However, for very small detunings, the two points appear stationary over several hundred oscillations, and then suddenly switch places, only to appear stationary again.

We were also able to observe, in agreement with theoretical predictions [12], that decreasing the detuning enhances the suppression of period doubling. Lastly, we remark that the effects of a rolling instability can be observed by comparing the time-series in figs. 7a and 10a: the presence of a rolling instability in the latter causes a larger uncertainty in the phase of impact.

5. Summary

This paper has addressed the problem of period doubling suppression via periodic (near-resonant) perturbations. We focussed on a particular physical system – the bouncing ball – which is amenable to both theoretical and experimental study.

Theoretically, we were able to perform an explicit center manifold reduction for the case where the table oscillates at two frequencies, the large-amplitude component having nearly twice the frequency of the perturbing component. In order for the analysis to parallel the usual procedure familiar from bifurcation theory, it was necessary to introduce a time-dependent center manifold. The resulting one-dimension equation for the dynamics on the center manifold agrees with the "normal form" of ref. 12. As anticipated, this normal form, eq. (1.2), is the continuous-time limit of the second iterate of the reduced Poincaré return map. In addition, our analysis leads to a new prediction governing the aspect ratio of the elongated ellipses traced out by iterates of the Poincaré map.

Our experiments focussed on two effects: the bifurcation point shift, and the dramatic "square-wave" nature of the output near the shifted bifurcation point. (Aside from electrical analog simulations [12], this represents the first experimental measurements on these phenomena; however, we emphasize that parallel experiments are being performed simultaneously by Pieranski and Malecki [36].) The "squaring" of the output for increasing perturbation strength is a qualitative effect which is easily observed (fig. 10). The bifurcation shift followed the 2/3-power law for perturbation amplitudes up to $\sim 4\%$ of the main driving amplitude – for larger perturbations our measurements suggest a crossover to another scaling regime with observed power law $\mu_* \propto \Lambda^{0.33 \pm .02}$. We have no formal theoretical explanation for this new behavior, though we suspect is may not be generic. For perturbations larger than $\sim 10\%$, the effects of higher periodic orbits – and even chaos – are evident, and complicate the dynamics beyond the scope of the low-order perturbation analysis of section 3.

The present study was motivated directly by the success of ref. 12, and represents an advance insofar as it carries out the scheme of fig. 3, rather than introducing the perturbation by hand after reducing the unperturbed dynamics. On the other hand, we studied a particular example only, whereas ref. 12 made a general analysis which suggested that the phenomena associated with near-resonant perturbations of period doubling bifurcations are generic. The next step, then, is to extend the present analysis to the general case.

Acknowledgements

We thank Neal Abraham, Al Albano, Paul Bryant, Bob Cawley, Richard Crandall, Tina Mello, N. Felsig Pedersen, Piotr Pieranski, Sheldon Newhouse, and Jim Yorke for use suggestions, and David Pine for the loan of two function generators. Work at Brookhaven National Laboratory was supported by Division of Materials Sciences U.S. Department of Energy under contract DE-AC02-CH00016.

References

[1] J. Heldstab, H. Thomas, T. Geisel and G. Radons, Z. Phys. B 50 (1983) 141.
[2] K. Wiesenfeld, J. Stat. Phys. 38 (1985) 1071; Phys. Rev. A 32 (1985) 1744.
[3] C.D. Jeffries and K. Wiesenfeld, Phys. Rev. A 31 (1985) 1077.
[4] P. Pieranski and J. Malecki, Phys. Rev. A 34 (1986) 582.
[5] K. Wiesenfeld and B. McNamara, Phys. Rev. Lett. 55 (1985) 13; Phys. Rev. A 33 (1986) 629.
[6] K. Wiesenfeld, Phys. Rev. A 33 (1986) 4026.
[7] O.H. Soerensen, J. Mygind and N.F. Pedersen, AIP Conf. Proc. 44 (1978) 246.
[8] J. Mygind, N.F. Pedersen and O.H. Soerensen, Appl. Phys. Lett. 32 (1978) 70.
[9] J. Mygind, N.F. Pedersen, O.H. Soerensen, B. Duelholm and M.T. Levinsen, Appl. Phys. Lett. 35 (1979) 91.
[10] H. Grothe, W. Harthe and P. Russer, Electron. Lett. 12 (1976) 522.
[11] B. Derighetti, M. Ravani, R. Stoop, P.F. Meier, E. Brun and R. Badii, Phys. Rev. Lett. 55 (1985) 1746.

[12] P. Bryant and K. Wiesenfeld, Phys. Rev. A 33 (1986) 2525.
[13] H. Savage and C. Adler, private communication.
[14] N.F. Pedersen, H. Svensmark and J.B. Hansen, Phys. Rev. A (to appear).
[15] J. Guckenheimer and P. Holmes, Nonlinear Oscillations, Dynamical Systems and Bifurcations of Vector Fields (Springer, New York, 1983).
[16] J.E. Marsden and M. McCracken, The Hopf Bifurcation and Its Applications (Springer, New York, 1976).
[17] J. Carr, Applications of the Center Manifold Theory (Springer, New York, 1981).
[18] P.J. Holmes, J. Sound Vib. 84 (1982) 173.
[19] P. Pieranski, J. Phys. (Paris) 44 (1983) 573.
[20] N.B. Tufillaro and A. Albano, Am. J. Phys. 54 (1986) 939.
[21] P. Pieranski, Z.J. Kowalik and M. Franaszek, J. Phys. (Paris) 46 (1985) 681.
[22] T.M. Mello and N.B. Tufillaro, Am. J. Phys. (in press).
[23] M. Franaszek and Z.J. Kowalik, Phys. Rev. A 33 (1986) 3508.
[24] N.B. Tufillaro, T.M. Mello, Y.M. Choi and A.M. Alabano, J. Phys. (Paris) 147 (1986) 1477.
[25] R.M. Everson, Physica 19D (1986) 355.
[26] M.J. Feldman, P.T. Parrish and R.Y. Chiao, J. Appl. Phys. 46 (1975) 4031.
[27] Y. Taur and P.L. Richards, J. Appl. Phys. 48 (1977) 1321.
[28] S. Martin and W. Martienssen, Phys. Rev. A 34 (1986) 4523.
[29] J. Yorke, private communication.
[30] See, e.g., H. Haken, Synergetics: An Introduction (Springer, New York, 1977).
[31] L.D. Pustylnikov, Trans. Moscow Math. Soc. 2 (1978) 1.
[32] E. Fermi, Phys. Rev. 75 (1949) 1169.
[33] The speaker size is not critical. We have built bouncing ball systems from speakers that range in size from 4″ to 15″.
[34] The KYNAR piezoelectric film is available from Pennwalt Corporation, 900 First Avenue, P.O. Box C, King of Prussia, PA 19046. A 10 cm × 20 cm sheet of 28 μm thick film with standard nickel–aluminum coating costs $35. The KYNAR Technical Manual is available from Pennwalt, and provides a wealth of applications as well as listing suppliers of conducting adhesives.
[35] We used the Bench Top Instrument (BEN-2048) with the analog subsystem (ADB12.16) available from Metaresearch, Inc., 1100 S.E. Woodward St., Portland, OR 97202. We controlled the Bench Top with the program "time-series" developed by R. Crandall of the RASCAL team, also available from Metaresearch.
[36] P. Pieranski and J. Malecki, unpublished.